Measurements and optimization of the occulting disk for the ASPIICS/PROBA-3 formation flying solar coronagraph

Measurements and optimization of the occulting disk for the ASPIICS/PROBA-3 formation flying solar coronagraph

Federico Landini[a], Alexandra Mazzoli[b], Mélanie Venet[c], Sebastien Vivés[c], Marco Romoli[a], Philippe Lamy[c], Guglielmo Rossi[d]

[a]Dipartimento di Fisica e Astronomia - Sezione di Astronomia, Università di Firenze, Largo Fermi 2, Firenze, Italy;
[b] Centre Spatial de Liège - Université de Liège, Av. du Pre-Aily, Liège, Belgium;
[c] Laboratoire d'Astrophysique de Marseille, rue Frèdèric Joliot-Curie, Marseille, France;
[d] Dipartimento di Scienze della Terra, Università di Firenze, Via la Pira 4, Firenze, Italy

ABSTRACT

Solar coronagraphs in formation flying require several mechanical and technological constraints to be met. One of the most critical issues is the external occulter design and its optimization. The occulter edge requires special attention in order to minimize the diffraction while being compatible with the constraints of handling and integrating large delicate space components. Moreover, it is practically impossible to realize a full scale model for laboratory tests. This article describes the results of tests performed with a scaled-model breadboard of the ASPIICS coronagraph disk edge, using the Artificial Sun facility at Laboratoire d'Astrophysique de Marseille.

Keywords: Coronagraph, external occulter, apodization, stray light, measurements, ASPIICS, formation flying

1. INTRODUCTION

The "Association de Satellites Pour l'Imagerie et l'Interferometrie de la Couronne Solaire", ASPIICS, selected by ESA for the PROBA 3 mission, heralds the next generation of coronagraph for solar research, exploiting formation flying to gain access to the inner corona under eclipse-like conditions for long periods of time. ASPIICS will observe the solar corona from 1.015 $R_\odot$ to ~ 3 $R_\odot$ in different modes:

- high spatial resolution imaging of the continuum K+F corona in photometric and polarimetric modes;
- high spatial resolution imaging of the E-corona in two coronal emission lines: Fe XIV 530.3 nm and He I D3;
- two-dimensional spectrophotometry of the Fe XIV emission line.

A more detailed description of the ASPIICS payload can be found in Lamy and Damé paper.[1]
ASPIICS is distributed on the two PROBA 3 spacecrafts (S/C) separated by 150 m. The coronagraph optical assembly is hosted by the "coronagraph S/C" protected from direct solar disk light by the occulting disk on the "occulter S/C". ASPIICS' optical design follows the general principles of a classical externally occulted Lyot coronagraph.[2]
The most critical issue in the design of a solar coronagraph is the reduction of the stray light due to the diffraction and scattering of the solar disk light from the optics. For ASPIICS, the complete stray light analysis is a complex issue that has been treated in a separate paper.[3]
In classical externally occulted coronagraphs a special care must be reserved to the occulting disk edge design and apodization. Putting an external disk to occult the solar disk induces a further problem in the stray light

Further author information: (Send correspondence to Federico Landini)
Federico Landini: E-mail: flandini@arcetri.astro.it, Telephone: 0039 055 205 5221

Ground-based and Airborne Instrumentation for Astronomy III, edited by Ian S. McLean, Suzanne K. Ramsay, Hideki Takami, Proc. of SPIE Vol. 7735, 77354D · © 2010 SPIE · CCC code: 0277-786X/10/$18 · doi: 10.1117/12.857541

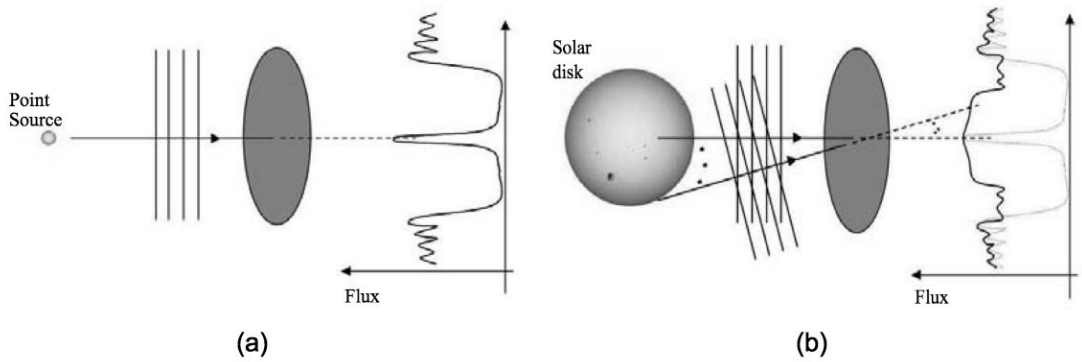

Figure 1. Sketches of the Poisson spot effect in the cases of a single on-axis source point (a) and of the whole solar disk (b).

issue: the Poisson spot. In fact, a plane wave impinging on a opaque disk produces a peak of diffracted flux just behind the disk, in correspondence of the intersection of the occulter symmetry axis with the image plane. If we imagine the solar disk as an infinite set of non-coherent point sources, we conclude that infinite non-coherent plane waves impinge on the occulter with different incident angles, producing a raised diffraction profile, as shown in figure 1.

The novelty of ASPIICS coronagraph concept (i.e., the coronagraph with the most Moon-like occulter ever built, in terms of both distance occulter-pupil and dimension) does not allow to rely completely on literature for apodization choice, since all space-borne coronagraphs that are accounted for are within ∼2 m of length, and all dimensions are scaled more or less accordingly. A dedicated study must be performed, several apodization systems have to be tested and compared together, both from a qualitative and a quantitative point of view.
This paper is devoted to the description of such an analysis, that has been performed within the ESA STAR-TIGER project devoted to formation flying coronagraphs. The first part of the paper is dedicated to the comparison among pros and cons of the apodization systems that can be found in literature, by considering their performances in stray light reduction and the issues connected with their possible implementation in the PROBA 3 mission. The second part of the paper is dedicated to the practical analysis, i.e., to the measurements we performed at the Laboratoire d'Astrophysique de Marseille in order to determine occulter apodization performances and manufacturing tolerances.

2. LITERATURE HERITAGE AND ASPIICS REQUIREMENTS

In the solar physics community there has been a long debate on the most efficient apodizing system for coronagraphic occulting systems. The three most discussed and used systems are (see figure 2): toothed disk, triple disk (in general multiple disks), multithreaded or polished frustum of a right cone (or barrel).

There are 5 milestone papers on the analysis of the apodization techniques; in chronological order, the main authors are: Newkirk,[4] Fort,[5] Lenskii,[6] Koutchmy,[7] Bout.[8] The only system theoretically fully analyzed is the toothed disk,[6] while the triple disk and the multi-thread solution are only qualitatively explained and experimentally tested. In particular, Koutchmy and Bout report an experimental and theoretical (where possible) comparison among the different apodizing systems.

2.1 Toothed disk

This method was first proposed by Purcell and Koomen in 1962,[9] and consists of a single disk with a serrated edge. The case has been theoretically analyzed by Lenskii,[6] and experimentally tested by Fort[5] and Koutchmy.[7] Figure 3 shows a sketch of the toothed disk design: the series of very tiny and sharp teeth is designed to spread diffracted light along the edge of the shadow of the disk itself, and not into the shadow (i.e. towards the objective). It is a very efficient solution, but complicate to achieve. The main challenge is to manufacture very

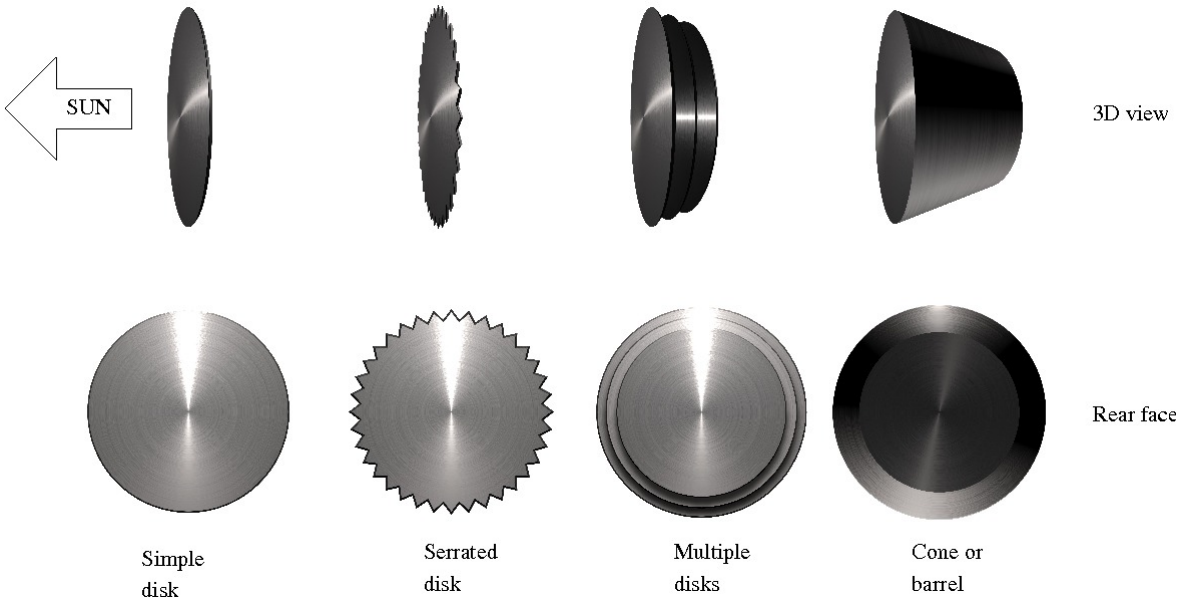

Figure 2. Summary of the most discussed and used apodizing systems in coronagraphy, compared with the simple disk.

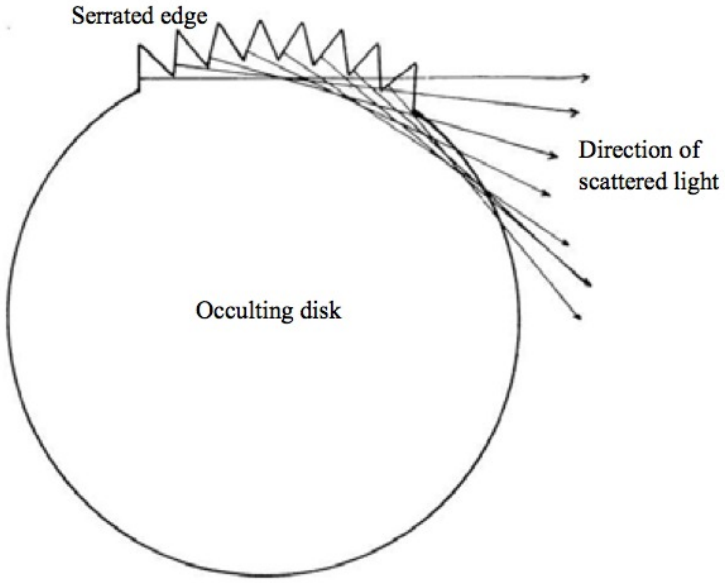

Figure 3. Sketch of the occulting disk with a serrated edge (courtesy of Tousey, 1965[10]).

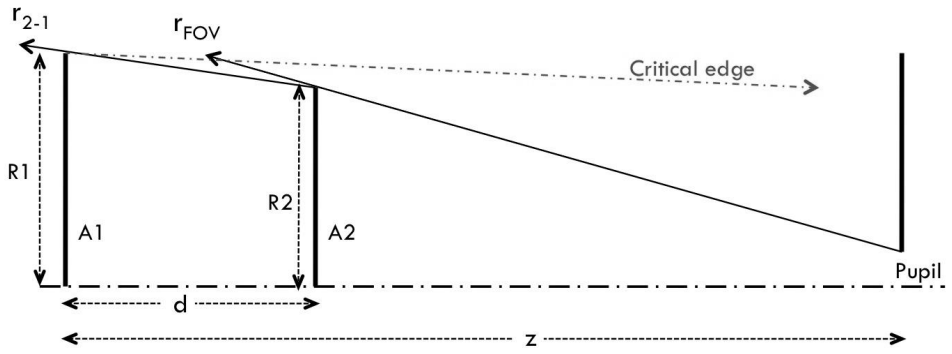

Figure 4. Drawing principle for a multiple disks system.

sharp teeth, that have to be very clean. Every single particle that settles down on the teeth or in the thin hollow between two successive teeth, can scatter light, and becomes a dangerous stray light source: scattering due to dust settling between two successive teeth can be limited by coupling two disks de-phased by half a tooth.
It has been used in several space-borne coronagraphic missions:

- 1963: a NRL team, leaded by R. Tousey, obtained the first image of the extended corona with a rocket flight.[10]
- 1968÷1970: A. Dollfus flew a coronagraph on a balloon.[11]
- 1993÷1998: the SPARTAN 201 mission flew an externally occulted coronagraph spectrometer with a toothed linear occulter to obtain the first UV observation of the extended solar corona.[12]
- 1995÷Now: SOHO-UVCS (Ultraviolet Coronagraph Spectrometer) uses the same design concept of the SPARTAN 201 instrument.[13]

2.2 Multiple disks

This system was first proposed and tested by Newkirk and Bohlin in 1963.[4] A second disk, in the shadow of the first, with respect to the solar disk, blocks the radiation diffracted by the first disk edge; a third disk, in the shadow of the second one, blocks the diffraction produced by the second disk edge, and so on. Actually, all flown coronagraphs using this solution mounted a 3-disks system. Figure 4 describes the drawing principle for a multiple disks system, by designing just two disks: d is the disks interdistance, z the distance between the external occulter and the entrance pupil of the coronagraph. For ASPIICS, z=150 m, $r_{FOV} = 1.015\ R_\odot$. If $r_{2-1} < r_{FOV}$ (and the same inequality holds also for successive disks), then the multiple disks system has a barrel profile, while if $r_{2-1} = r_{FOV}$ then the profile is conic. The conic occulter, described in section 2.3, is designed following this principle.
Lenskii[6] performs an analysis of the stray light level behind a two-disks system, and extends the result to infer an estimate of the stray light level behind a three-disks system, but without a proper theoretical analysis.
This system has been adopted by:

- 1965: the balloon-borne Coronascope II of Newkirk and Bohlin.[14]
- 1971÷1974: the white light coronagraph in OSO-7.[15]
- 1995÷Now: LASCO-C3 aboard SOHO,[16] that is producing visible light images of the extended solar corona up to 30 $R_\odot$.
- 2006÷Now: Cor2 coronagraph of the STEREO/SECCHI mission.[17]

- 2009: HERSCHEL/SCORE[18] and HERSCHEL/HeCor[19] coronagraphs, the first two coronagraphs that observed the extended corona in the HeII 30.4 nm line.

Laboratory tests for the GOES-R coronagraph occulter, even if conducted for a multiple disk system, demonstrated that for compact coronagraphs the barrel design is preferable to the cone profile.[20]

2.3 Cone or barrel

The multi-threaded cone or barrel is the logical extension of the three-disks system; it is basically an improvement of the number of disks, each one in the shadow of the previous, and each one blocking the light diffracted by the previous disk edge. The idea was proposed by Newkirk and Bohlin, but they did not consider this solution very much reliable, because of the "inevitable irregularities in the disk" that "throw spurious radiation into the objective aperture".[4] This result was overturned by Koutchmy and Belmahdi experimental tests in 1987.[21] LASCO-C2 aboard SOHO is using this solution with excellent results.[16]
By increasing the number of disks to infinity, we get a polished cone or barrel, that has been compared with the multi-thread solution only by Bout.[8]

2.4 ASPIICS requirements

ASPIICS inner field of view is 1.015 $R_\odot$. This constraint forces us to drop the toothed disk as possible apodized occulter. In fact, even by using a tiny peak-to-valley distance of 0.5 cm (that would mean a number of teeth of about 5000 and a peak-to-peak distance of 50 μm) the FOV would be increased to 1.02 $R_\odot$.
The pointing stability is another requirement that has to be matched: the spacecraft must keep the alignment within strict tolerances. This constraint suggests not to adopt long apodizing systems, such as the multiple disks system, but also a cone or barrel should be very compact along the optical axis, i.e. $\sim 10 \div 15$ cm.
In order to support this statement, we performed a simple simulation, comparing together the performances of different instruments with a two disks occulter. Figure 5 shows the result. The y-axis of the plot represents the ratio I_2/I_1, where I_2 is the normalized diffracted flux on axis on the entrance pupil plane behind a two-disks system, and I_1 is the same quantity for a single disk. Both values are calculated with the whole solar disk as a source and are given by formulas (8) and (6), respectively, from Lenskii paper.[6]
Three instrument are compared together: STEREO-SECCHI/Cor2, HERSCHEL/SCORE and ASPIICS. The x-axis is different for each instrument, since they have different dimensions.
Both Cor2 and SCORE disks interdistance were not chosen by using these simulations, nevertheless this plot is an evidence to support the goodness of those choices. The interdistance of two disks is 25 cm for SCORE and 5 cm for Cor2. Both distances roughly correspond to the range where simulated curves slope starts smoothing. Moving disks further beyond that range would not bring the same improvement in stray light reduction as for shorter interdistances. If we imagine to apply the same principle to ASPIICS, we would need a spindle of at least 5 meters to hold two disks with one order of magnitude less stray light reduction with respect to Cor2 and SCORE. This is due to ASPIICS small inner FOV and to the huge dimension of the coronagraph (1.5 m diameter occulting disk, 150 m far from the entrance aperture).
As a rule of thumb, also the conic occulter should keep the same dimensions of the multiple disk system, since they share the same design principle (see figure 4). But a conic occulter has never been simulated, so previous statement cannot be confirmed. Moreover, if we consider a conic surface (or barrel) and not a multi-thread with a conic profile (or barrel), also the material and the surface finishing can affect the performances. Laboratory tests have been performed in order to track a path in this still unexplored area.
Since a polished or electro-eroded cone (or barrel) is more easily achievable and less expensive than a multi-threaded one, we decide to drop the multi-thread possibility and concentrate on apodizing surfaces, also because, according to literature,[8] they have comparable performances.
Figure 6 shows that if we draw a barrel following the same principle that we use for a multiple disk system (see figure 4), then over a length of 15 cm we get $R_c - R_b \sim 4$ μm, that means that cone or barrel have the same shape within the manufacturing tolerances. A possibility is to investigate compact barrels with different design principles (see section 4.4).

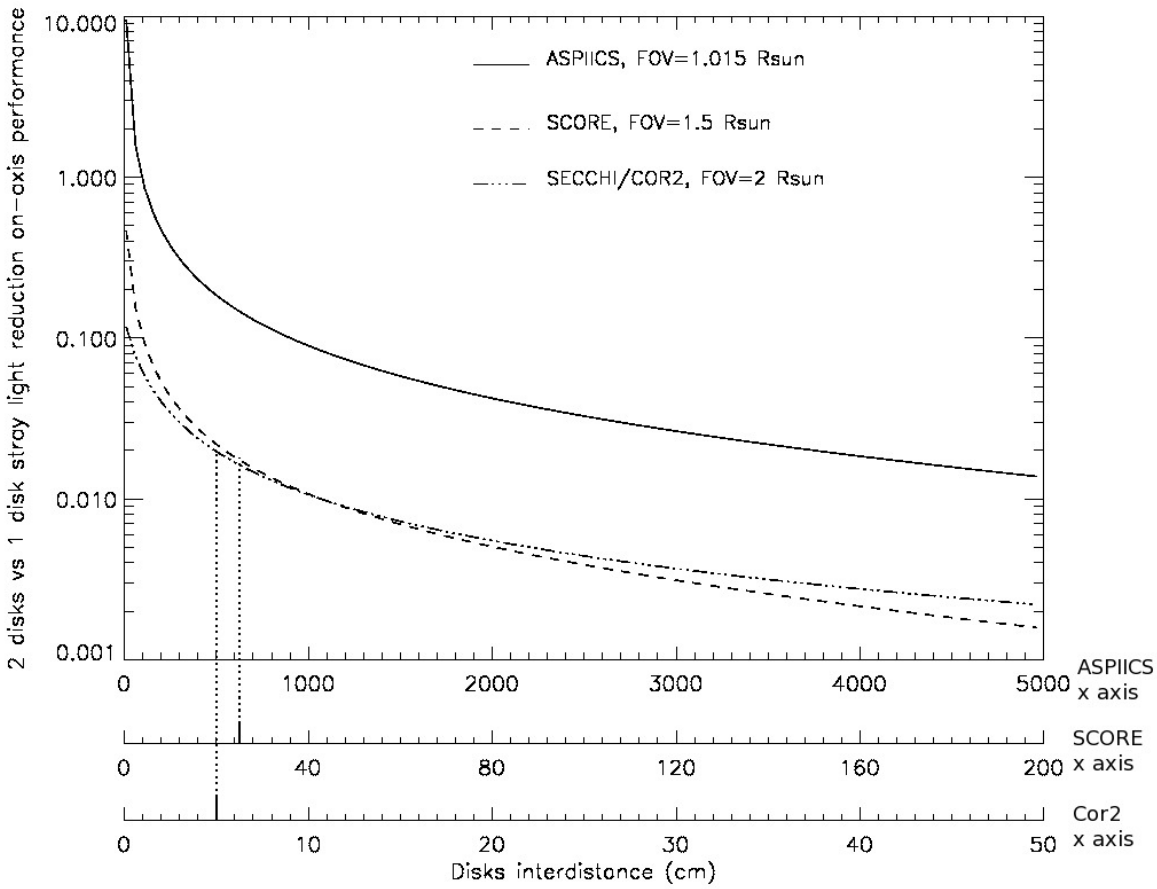

Figure 5. Stray light reduction performances as a function of two occulting disks interdistance: comparison among different coronagraphs.

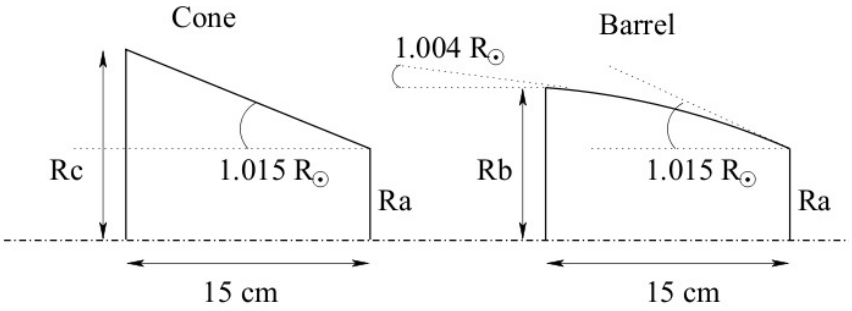

Figure 6. Cone geometry compared to barrel: if we follow the same principle in designing the two apodizations (see figure 4), given the flight geometry, differences are negligible ($R_c - R_b \sim 4$ μm).

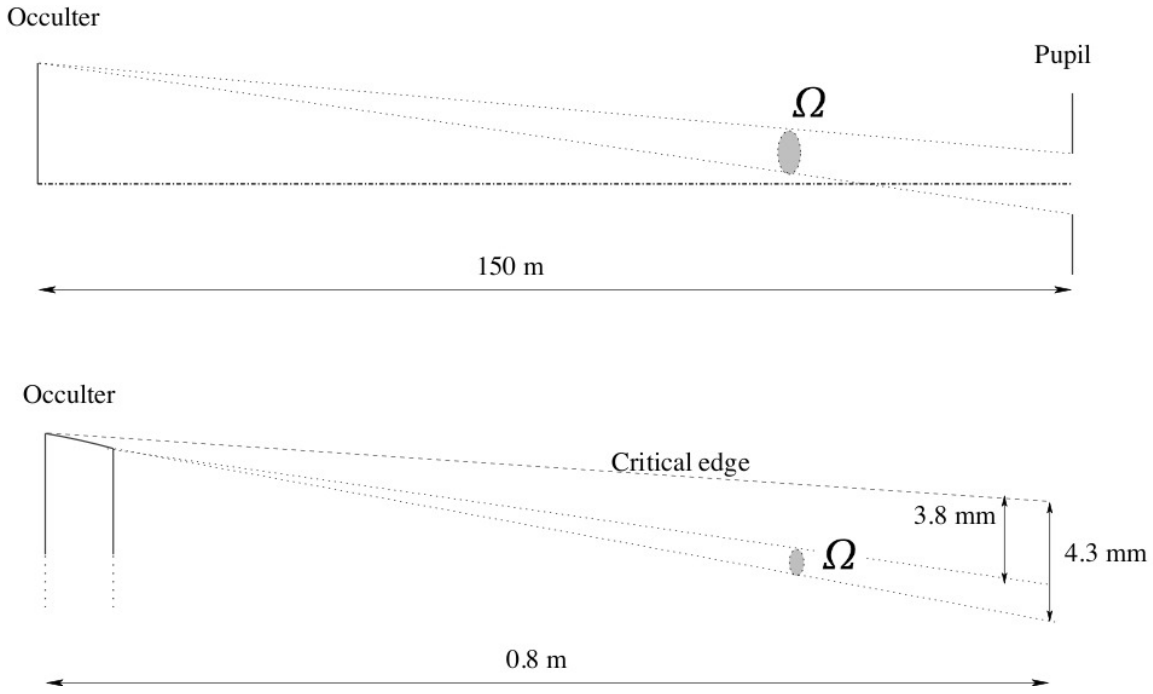

Figure 7. Comparison between flight (up) and laboratory (down) configurations. The critical edge is defined by the ray coming from the solar limb.

3. LABORATORY SET-UP

A tests set-up has been designed and realized at the Laboratoire d'Astrophysique de Marseille (France), within a class 100 clean room. A solar simulator has been used as source. A description of a similar source can be found in Bout et al. paper.[8]

Since it is practically impossible to realize a full-scale model for laboratory tests, we designed a test set-up able to measure the stray light behind a section of the whole occulter. The section of such a large occulter (1.5 m diameter) can be well approximated by a small straight edge occulter. It is reasonable to measure the stray light pattern behind the occulter in the same solid angle defined by the space real-model geometry. Figure 7 shows a comparison between laboratory and flight geometries. The stray light we are interested in is the portion of all the light scattered by the occulter edge that is collected by the telescope entrance pupil. So we have to measure the stray light pattern in the solid angle Ω subtended by the pupil as seen by the occulter edge (figure 7 top). This creates some challenging issues in the laboratory configuration, since we have to measure the stray light pattern very near to the solar disk critical edge (figure 7 bottom), that is defined by the ray coming from the solar limb, grazing the occulter edge.

Since we are measuring the diffraction pattern behind a linear occulter and not behind a disk, it is not possible to extrapolate directly the result we obtain to the flight model of the coronagraph. On the other hand it is possible to perform a relative analysis, by comparing stray light reduction performances of the apodized linear occulters with the razor edge.

The light diffracted from a razor edge, being easily computable even for an extended source (see section 4.1), is the reference for all the sets of measurements. A sketch of the measurement set-up is represented in figure 8. A complete overview of the set-up is shown in figure 8 (a): the source is a collimator that simulates the angular aperture of the real solar disk. Light from the source enters the class 100 clean room through an aperture. In the clean room, the stray light measurement set-up is assembled. The detector is a photodiode (Newport 818-SL), with a baffle mounted in front. The baffle holds a 0.45 mm pin-hole, to allow a high resolution sampling.

A light trap is placed very near to the detector, in order to prevent direct "solar" disk light from being scattered everywhere inside the room.

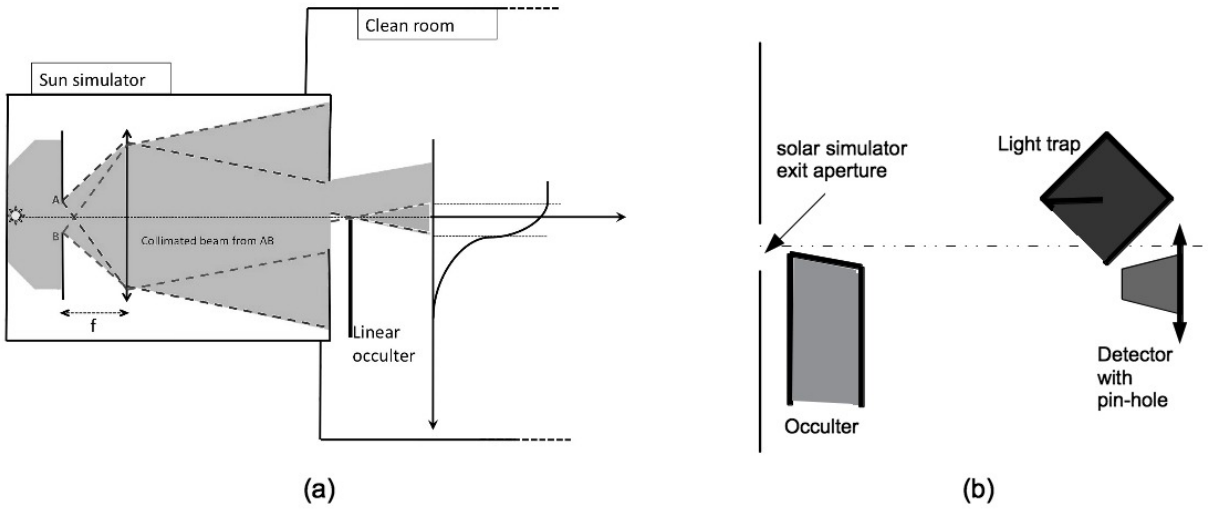

Figure 8. Sketch of the measurement set-up. (a) Overview of the complete set-up, divided in two separated rooms, communicating only by the exit aperture of the source. (b) Particular of the optics set-up for stray light measurement behind the occulter.

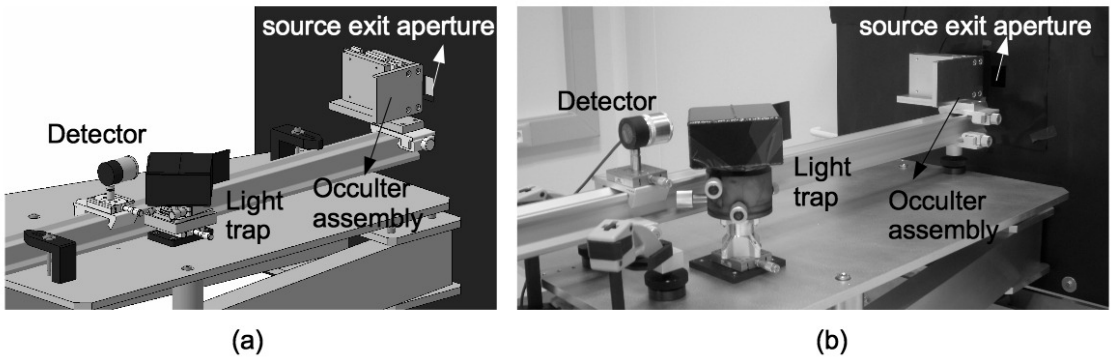

Figure 9. (a) technical design of the whole measurement setup; (b) picture of the actual realization.

Stray light measurements are performed behind the linear occulter along a direction perpendicular to the occulter edge.
All measurements are relative to the source unobstructed flux (i.e., without occulter mounted).
In order to achieve the conic angle of the apodized linear occulter, we used a metal plate mounted on a precision steel tilting platform (Newport TGN-80). This also allowed us to define the tolerance we can afford in manufacturing the conic apodization, by repeating the stray light measurement behind the occulter for several conic angles (i.e., several tilting platform tilts). Figure 9 shows an overview of the designed measurement set-up (a), compared with the real one (b).

4. MEASUREMENTS

4.1 Razor edge: theory

The diffraction pattern behind a linear occulter is a relatively easy computation, even considering an extended source like the solar disk.
Using the well known Huygens-Fresnel theory,[22] the normalized diffracted light intensity pattern behind a razor

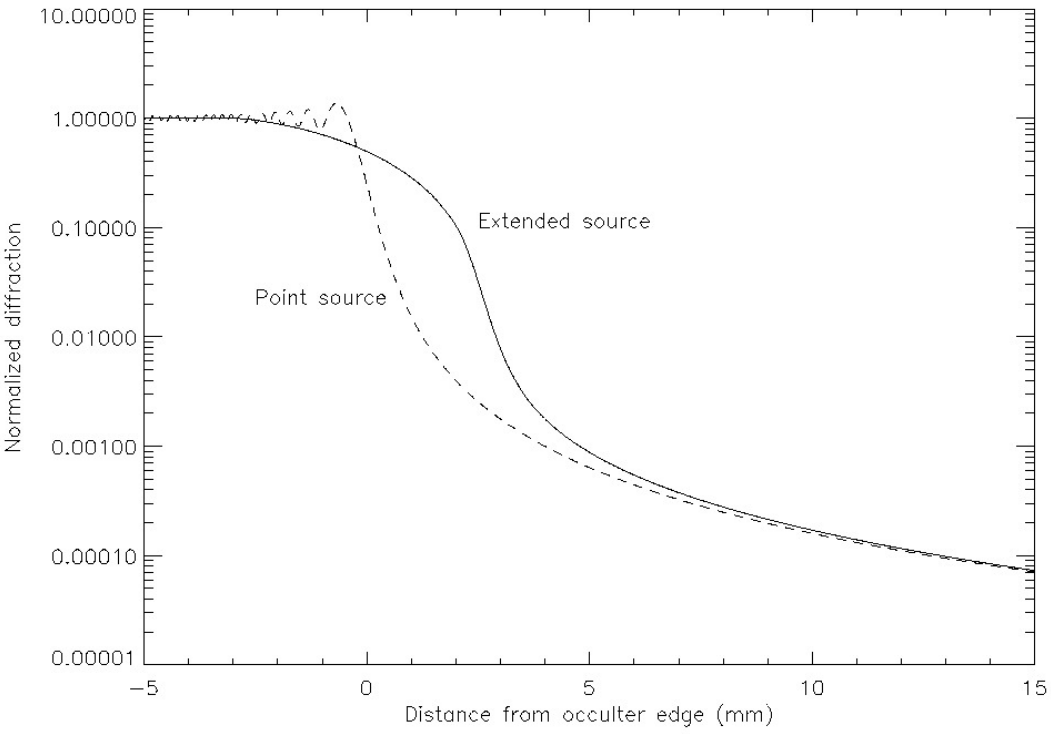

Figure 10. Theoretic diffraction behind a razor edge in case of point source at infinity (dashed line) and extended source (solid line).

edge for a point source at infinity is given by:

$$I(x,\lambda) = \left| \frac{1}{2} \left[(C(\alpha) - S(\alpha)) + i \ \ (1 + C(\alpha) + S(\alpha)) \right] \right|^2 \tag{1}$$

where λ is the wavelength, x is the coordinate on the image plane along the direction perpendicular to the occulter edge, $\alpha = x\sqrt{2/(\lambda L)}$, with L distance between the occulter and the image plane, i is the imaginary unit and $C(\alpha)$, $S(\alpha)$ are the Fresnel integrals.
By integrating equation (1) over the solar disk, after some brief analytical calculation, we get:

$$I_S(x,\lambda) = \frac{1}{\pi R_\odot^2} \int_{-R_\odot+x}^{R_\odot+x} \left\{ \left(\frac{1}{2} + C(\alpha_S) \right)^2 + \left(\frac{1}{2} + S(\alpha_S) \right)^2 \right\} B(x_S) dx_S \tag{2}$$

where x_S is the coordinate along the solar disk radius, $\alpha_S = \sqrt{2/(\lambda L)}(x - x_S)$ and $B(x_S) = \sqrt{R_\odot^2 - (x_S - x)^2}$
Figure 10 compares the diffraction given by equations (1) and (2). The 0 of the x-axis corresponds to the point where the line defined by the center of the Sun and the center of the occulter edge intersects the image plane. It can be interesting to note that we can easily recognize the pen-umbra and umbra (i.e., diffraction) zones in the curves. The inflection point on the descent defines the border between umbra and pen-umbra, in fact in correspondence of that point the light abruptly changes its decreasing slope.

4.2 Razor edge: measurement

With the set-up described in section 3, we performed a measurement in order to check the agreement of the measured diffraction pattern behind the razor edge and the signal foreseen by equation (2). Figure 11 shows a very good agreement between theory and measurements, thus confirming the reliability of the experimental set-up. The diffracted light behind a razor edge constitutes the reference for all our successive tests.

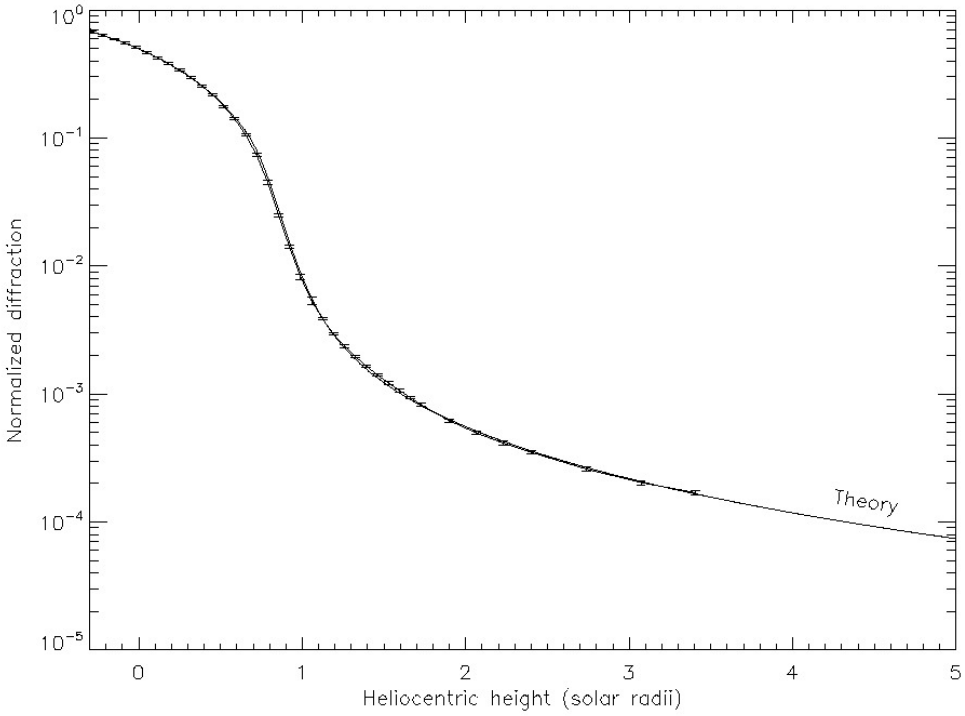

Figure 11. Measurements of diffracted light behind a razor edge occulter compared with theoretical curve, that will be shown in all plots.

4.3 Cone

With the set-up described in section 3, various conic apodizing configurations have been applied to the linear occulter. The longitudinal dimension of the cone is only one of the issues to be investigated in our tests. In order to understand how materials, surface polishing, scratches and assembling errors affect the stray light reduction performances of the apodized occulter, we performed several indicative tests, for each of which a different occulter was designed and manufactured.

A1 : Aluminum, 10 cm long, surface roughness σ=0.4 μm, that is the reference for all the tests.

A2 : Aluminum, 15 cm long, σ=0.4 μm, in order to investigate how length affects performances.

I1 : Invar, 10 cm long, σ=0.4 μm, in order to compare different materials performances.

A3 : Aluminum, 10 cm long, σ=0.4 μm, separated in two equal parts, A3G and A3D, in order to test if there are differences in stray light reduction performances between an occulter manufactured as one piece and an assembled one.

A4 : Aluminum, 10 cm long, σ=6.4 μm, in order to check whether a different surface finishing affects occulter performances.

A1s : a spare of A1, to be scratched on the surface at different depths: 20 μm and 200 μm, in order to check at which level scratches start to affect occulter performances.

Laboratory tests reveal that there is no difference in stray light reduction among A1, I1, A4 (not shown). This suggests that neither cone material nor its surface finishing affect stray light reduction performances. Figure 12 reveals that the conic apodization does indeed improve stray light performances with respect to the simple

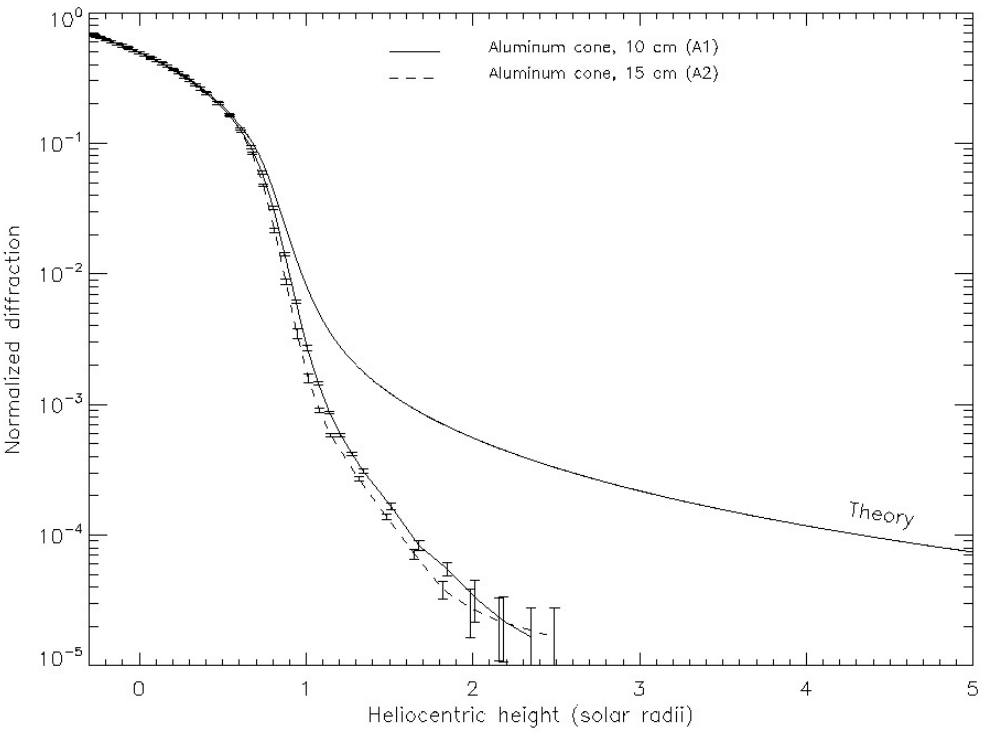

Figure 12. Comparison among A1, A2 and the theoretical razor edge curve.

razor edge. Moreover, an increase in the occulter longitudinal length (i.e., along the optical axis) improves the performances even more, as it is evident from the comparison between A1 and A2. This was somehow expected, as the ideal conic apodization for the ASPIICS occulting disk should be much longer than 15 cm, according to the design principle exposed in section 2.2 and to the comment in section 2.4.

Figure 13 shows that in case the conic is assembled we have no impact on the stray light reduction performances whether eventual assembling errors are made in the longitudinal direction, while we completely jeopardize the apodization effect in case of radial assembling errors. Tests were made by bad assembling A3G and A3D on purpose: the mistake in longitudinal alignment was 1.5 mm, while the radial misalignment was 0.5 mm. Figure 14 describes how scratches influence the performance of the apodized occulter. Skratches were realized with a drill, in two successive steps, on A1s surface.

- First step: scratches 20 μm deep.
- Second step: the surface was polished again and then scratches 200 μm deep were tracked.

This result allows us to establish that scratches at least 20 μm deep do not affect stray light reduction performances of the apodized occulter surface.

Finally, as far as a conic apodization is concerned, we established that in manufacturing the cone angle we have a tolerance of ~ 2 arcmin: we performed several measures by changing the angle defined by the tilting platform on which the apodizing metal plate was mounted, in order to simulate a different cone angle for each measurement. We got a deviation from the nominal behaviour, obtained with a cone angle of 34.05 arcmin (case of A1 in figure 12), only beyond 36 arcmin.

4.4 Toroidal occulters

In section 2.4 we noticed that designing a barrel with the principle of figure 4, due to ASPIICS geometry we cannot deviate appreciably from a cone. In any case, we can change arbitrarily the barrel designing principle, and

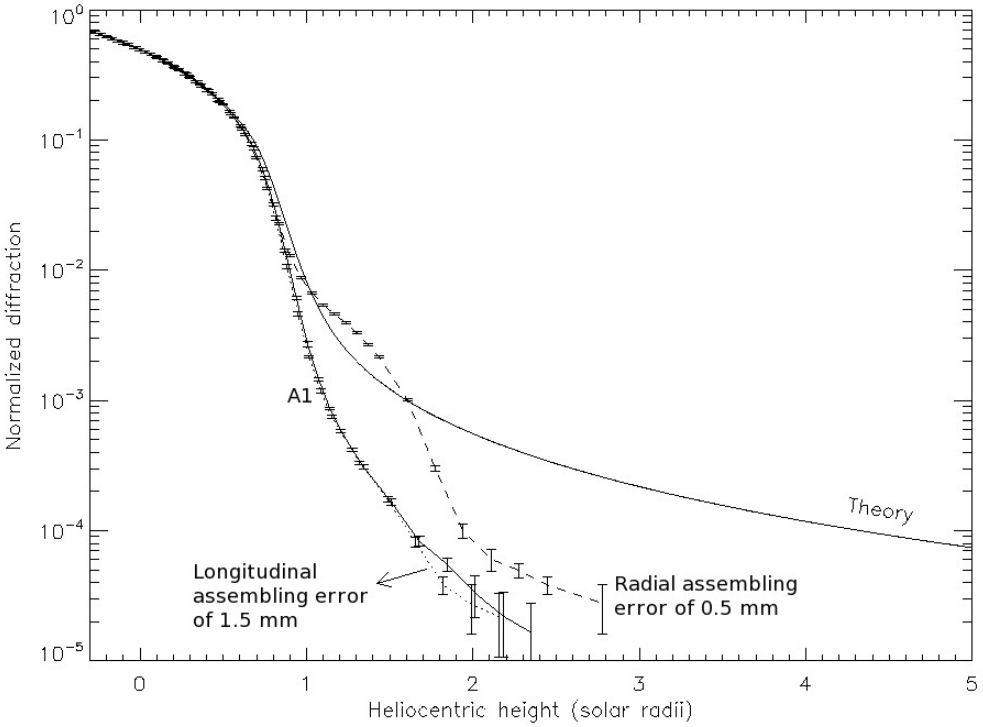

Figure 13. In case of assembled cone, radial assembling errors deeply affect apodization performances, while longitudinal assembling errors are practically uneffective.

compare its performances with the conic occulter. We designed three different linear occulters with a cylinder-like geometry, that if extended on ASPIICS external occulter profile give rise to toroidal occulters.
These occulters differ for the radius of curvature. In order to investigate the widest possible field of geometries we choose to adopt 1 cm, 10 cm, 1 m as radii. Figure 15 shows the three manufactured occulters, together with a 3D drawing of the 1 cm occulter mounted in the set-up and a sketch showing the curvature radius definition. All the three toroidal occulters were made by electro-eroded Aluminum.
Figure 16 shows the results of the three toroidal occulters compared with A1. The 1 cm toroidal occulter is the worst of the three, and performances increase by flattening the surface. 100 cm radius occulter, that is in fact almost flat, has a behaviour comparable with the conic occulter. On the other hand, sensitivity to occulter tilt is negligible for the 1 cm toroid, and is the same of A1 for the 100 cm one.

5. CONCLUSIONS

A trade-off study was performed for the 1.5 m diameter external occulter of the ASPIICS coronagraph, selected for the formation flight PROBA3 ESA mission. The analysis was both qualitative (based upon literature theoretical and laboratory descriptions) and quantitative. In fact, several sets of measurements were performed at the Laboratoire d'Astrophysique de Marseille (France), with a set-up mounted in a class 100 clean room and using a solar simulator source. Since it is impossible to replicate in laboratory the flight configuration, due to the huge dimensions of the involved instruments, we designed a set-up to test the stray light performances of just a portion of the big occulting disk, that is well approximated by a linear occulter. All our results are relative to the unobstructed flux and to the razor edge stray light reduction performances. The result of our analysis is that an apodization improves the stray light reduction performances of a simple disk, and that a conic apodization is the best solution, even if the cone has to be very compact along the optical axis. Our analysis shows also that such a system is relatively insensitive to tilt (within 2 arcmin) and scratches (at least 20 μm deep) on the conic

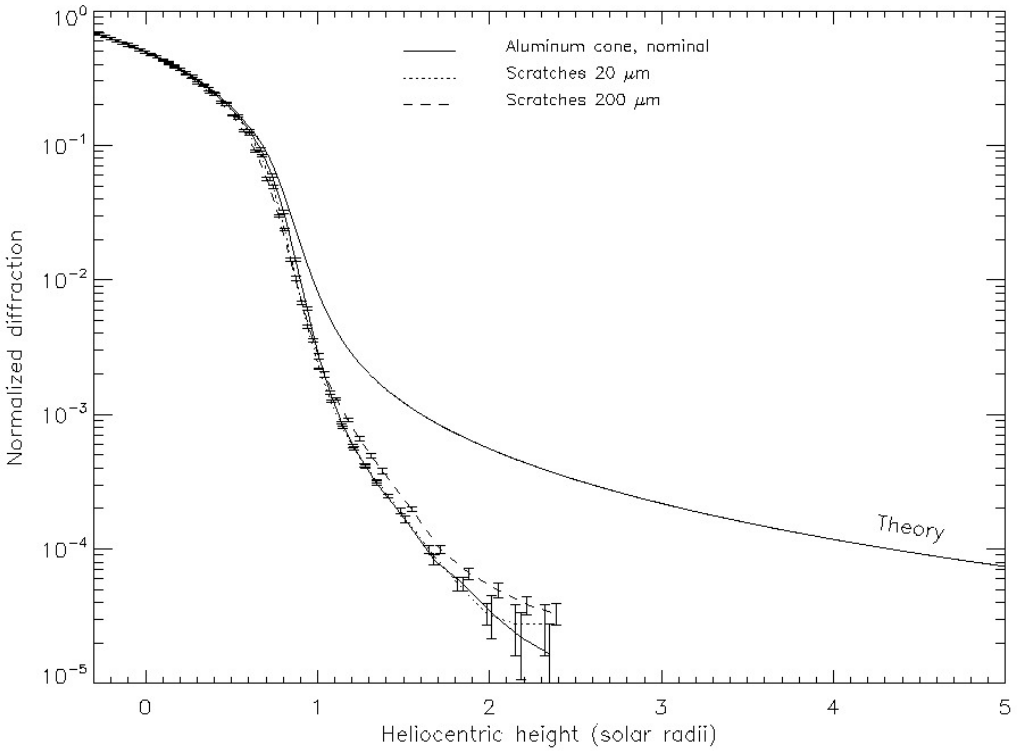

Figure 14. Comparison among two types of A1s scratched surfaces and A1 (with no scratches).

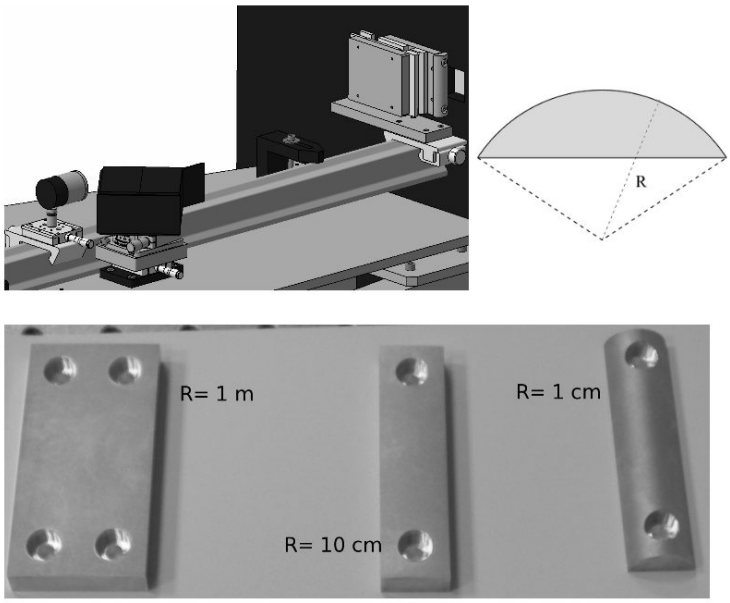

Figure 15. Clockwise, from the top left: 3D drawing showing the 1 cm radius occulter mounted in the set-up; sketch showing a section of the toroidal occulter, in order to define the curvature radius R; picture of the three manufactured toroidal occulters.

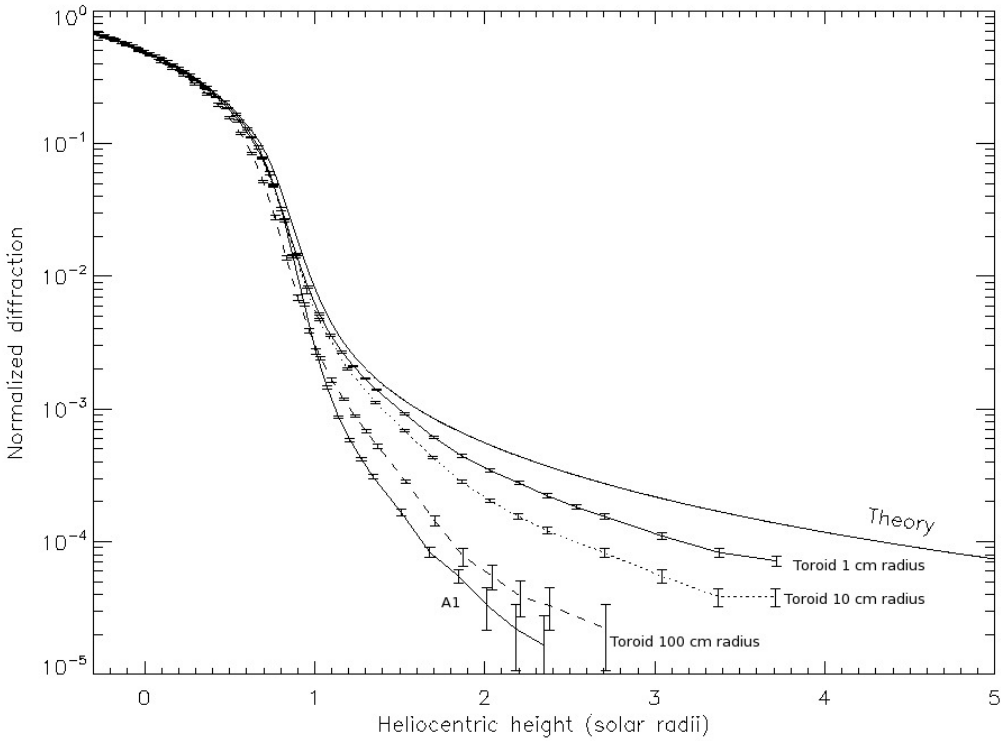

Figure 16. Comparison among the three toroidal occulters, A1 and the theoretical razor edge curve.

surface. The cone has to be as long as possible, in order to improve its efficiency. We tested also some toroidal apodizations, that are less efficient than the conic ones.

ACKNOWLEDGMENTS

This work could not have been completed without the help of Giuseppe Massone of INAF-Osservatorio Astronomico di Torino, that designed and manufactured the baffle for the photodiode assembly, Christophe Guillon of LAM, that is the author of all the technical drawings of pieces to be manufactured, and José Garcia, responsible of all the work at LAM machine workshop.
This work was supported by the ESA fundings in the framework of the STARTIGER program.

REFERENCES

[1] Lamy, P. and Damé, L., "ASPIICS: a giant coronagraph for the ESA/PROBA-3 Formation Flying Mission," in [*Space Telescopes and Instrumentation 2010: Optical, Infrared, and Millimeter Wave*], *Proc. SPIE* **7731**, in press (2010).

[2] Evans, J. W., "Photometer for measurement of sky brightness near the sun," *J. Opt. Soc. Am.* **38**, 1083 (1948).

[3] Mazzoli, A., Landini, F., Vives, S., Lamy, P., Halain, J., and Rochus, P., "Stray light analysis and optimization of the ASPIICS/PROBA-3 formation flying solar coronagraph," in [*Space Telescopes and Instrumentation 2010: Optical, Infrared, and Millimeter Wave*], *Proc. SPIE* **7731**, in press (2010).

[4] Newkirk, Jr., G. and Bohlin, D., "Reduction of scattered light in the coronagraph," *App. Opt.* **2**(2), 131–140 (1963).

[5] Fort, B. et al., "The reduction of scattered light in an external occulting disk coronagraph," *A&A* **63**, 243–246 (1978).

[6] Lenskii, A. V., "Theoretical evaluation of the efficiency of external occulting systems for coronagraphs," *Sov. Astron.* **25**(3), 366–372 (1981).
[7] Koutchmy, S., "Space born coronagraphy," *Sp. Sc. Rev.* **47**, 95–143 (1988).
[8] Bout, M. et al., "Experimental study of external occulters for the Large Angle and Spectrometric Coronagraph 2: LASCO-C2," *App. Opt.* **39**(22), 3955–3962 (2000).
[9] Purcell, J. D. and Koomen, M. J., "Coronagraph with improved scattered-light properties," *J. Opt. Soc. Am.* **52**, 596 (1962).
[10] Tousey, R., "Observations of the white light corona by rocket," *Ann. d'Astr.* **28**, 600 (1965).
[11] Dollfus, A., "La couronne solaire vue de ballon," *L'Astronomie* **82**, 284 (1968).
[12] Kohl, J. L., Gardner, L. D., Strachan, L., and Hassler, D. M., "Ultraviolet spectroscopy of the extended solar corona during the SPARTAN 201 mission," *Sp. Sc. Rev.* **70**, 253–261 (1994).
[13] Kohl, J. L. et al., "The Ultraviolet Coronagraph Spectrometer for the Solar and Heliospheric Observatory," *Sol. Ph.* **162**, 313 (1995).
[14] Newkirk, Jr., G. and Bohlin, D., "Coronascope II: observation of the white light corona from a stratospheric balloon," *Int. As. Un. Symposium* **23**, 287–291 (1965).
[15] Koomen, M. J. et al., "White light coronagraph in OSO-7," *App. Opt.* **14**(3), 743–751 (1975).
[16] Brueckner, G. E. et al., "The Large Angle Spectroscopic Coronagraph (LASCO)," *Sol. Ph.* **162**, 357–400 (1995).
[17] Howard, R. A. et al., "Sun Earth Connection Coronal and Heliospheric Investigation (SECCHI)," *Sp. Sc. Rev.* **136**, 67–115 (2008).
[18] Romoli, M. et al., "The Ultraviolet and Visible-light Coronagraph of the HERSCHEL experiment," in [*Solar Wind Ten*], **679**, 846–849 (2003).
[19] Auchère, F. et al., "HECOR: a HElium CORonagraphy aboard the Herschel sounding rocket," *Proc. SPIE* **6689** (2007).
[20] Thernisien, A. et al., "Experimental and numerical optimization of a coronagraph external occulter. Application to SECCHI-COR2 and GOES-R SCOR," in [*Solar Physics and Space Weather Instrumentation*], Fineschi, S. and Viereck, R. A., eds., *Proc. SPIE* **5901**, 366–376 (2005).
[21] Koutchmy, S. and Belmahdi, M., "Improved measurements of scattered light level behind occulting systems," *J. Op.* **18**, 265–269 (1987).
[22] Born, M. and Wolf, E., [*Principles of Optics*], Cambridge University Press, Cambridge (2001).